ORIGINAL ARTICLE

Shear transfer at the steel-concrete interface using different mechanical connectors

Teodora Bogdan[1] | Herve Degee[2] | Dan Dragan[2]| Renata Obiala[3]

Correspondence

Dr. Teodora Bogdan
AMSFCE, FSTC, RUES, University of Luxembourg, Luxembourg
Email: teodora.bogdan@uni.lu

[1] ArcelorMittal Chair of Steel and Façade Engineering, FSTC, RUES, University of Luxembourg, Luxembourg
[2] FET, CERG, Hasselt University, Hasselt, Belgium
[3] ArcelorMittal Global R&D – Department of Construction and Infrastructure Applications, Esch sur Alzette, Luxembourg

Abstract

The present article is dealing with an assessment of the longitudinal shear at the steel-concrete interface using several types of mechanical connections. Experimental and numerical tests have been performed to understand better the short and long-term effects of the influence of the newly defined connectors.

Experimental tests consisted of 12-column push-out tests (CoPOT). In the test campaign, four types of surface finishing have been tested: i) reference tests (0v2) without any mechanical shear connectors, (ii) angled, V-shaped, variant of the novel flat shear connector (Av2), (iii) transversal variant of the novel flat shear connector (Bv2) and (iv) multiple ribs on the flanges having a height of 0.7mm (Cv2). Three specimens for each were tested in short-term loading. The loading procedure defined in EN1994-1-1:2004 Annex B was applied for all tests. Also, one of each specimen was tested in long-term loading to observe the effect of concrete shrinkage on the quality of bond properties. No significant differences were observed between both load phases and the test results after shrinkage fall in the margin of variation of short-term tests. Numerical simulations performed in FE code Abaqus® supported the investigation, using a simplified definition of the bond.

Keywords

steel-concrete composite column, longitudinal shear, push-out tests with fully embedded steel profiles, numerical finite element model of the steel-concrete

1 Introduction

Concrete-encased composite (CEC) columns have advantages over other structural components such as high bearing capacity, excellent stiffness, good ductility, height tenacity, and pronounced seismic resistance. The optimal use of steel and concrete requires shear connections at the interface of the materials.

Bond slip investigations between steel profiles and concrete have been carried out over the past decades. An adequate bond between steel and concrete is required although it is typically neglected in the design. Headed shear connectors are typically used in composite columns to enhance the connection between concrete and steel components. The type of shear connection between steel and concrete has a significant effect on the behaviour of composite members.

The behavior of headed stud connectors in solid concrete slabs has been comprehensively investigated [1], where their application for anchor plates in reinforcement concrete structures [2] and in chambers of encased steel profiles in composite columns [3] can be also recognized. Minor usage of other types of shear connectors can be identified, like welded stiffeners between the flanges of steel profiles [4], channel sections [5], perfobond solution [6], bearing plate connectors in filled hollow sections [7] and checkered steel plate pattern om the profile's flanges [8]. However, the available solutions on the market have been mainly developed for composite beams and have only been adapted for composite columns.

This paper aims to replace the classical shear connectors with novel shear connector types dedicated to overtaking the shear force transfer. Three distinct steel flange surface treatments are considered, as shown in Fig. 1. The I-shape and V-shape ribs have 8 mm rib height each. They are placed on the steel flange by using a WAAM process. The ribbed surface has a height of 0.7 mm and considers the maximum height that can be produced in the last rolling step.

The shear force transfer in composite members is experimentally measured using different techniques. The push-out test is the most common procedure because of its simplicity. This paper presents the experimental campaign of

12 push-out specimens of concrete-encased steel reinforced concrete sections submitted to short- and long-term loading [9]. The goal was to study the longitudinal shear performance of different interlocks in short and long-term effects. The acquired results have been implemented into Abaqus numerical models and calibrated with the experimental campaign. The purpose is later on to define a correlation between the rib height and the shape of the steel profile.

2 Experimental campaign

Within POT, the HE200B steel profile is embedded in the concrete cross-section of 400 mm x 400 mm. Longitudinal rebars 4 ϕ 16 have a concrete cover of 25mm, while the transversal rebars are ϕ8/150 mm. The reinforcement cage remains constant for all the tested specimens, as shown in Fig. 1. The dimension and geometry of the rib pattern as well as the loading procedure were selected as experimental parameters. The concrete test curve measured on the testing day had an average compressive strength of 35.2 N (C30/C37) while the steel profile grade is S355.

Four types of surface finishing have been tested: normal surface finishing – reference tests, V-shaped printed ribs on the flanges, I-shaped printed ribs on the flanges, perpendicular to the longitudinal axes of the profile and multiple ribs on the flanges of a height of 0,7mm. Each configuration contains 4 specimens.

The surface finishing dimensions and geometry has been chosen considering the ease of manufacturing. The ribs in I and V shape were previously studied by Chrzanowski [10], while the ribbed surface was meant to be placed in the last rolling step of the steel beam. All configurations were predefined using the procedure in Plumier [11] and meant to have the equivalent bearing capacity as the classical shear stud.

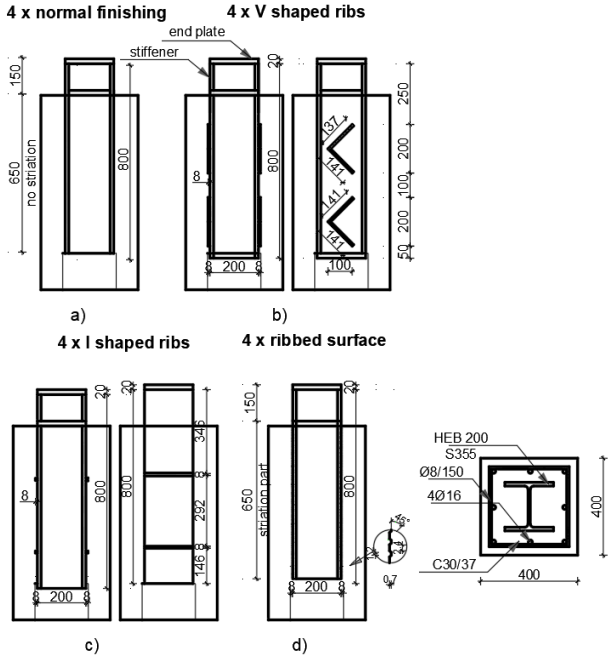

Figure 1 Overview of the column push-out test series: a) normal surface finishing, b) V-shaped ribs, c) I-shaped ribs, and d) ribbed surface.

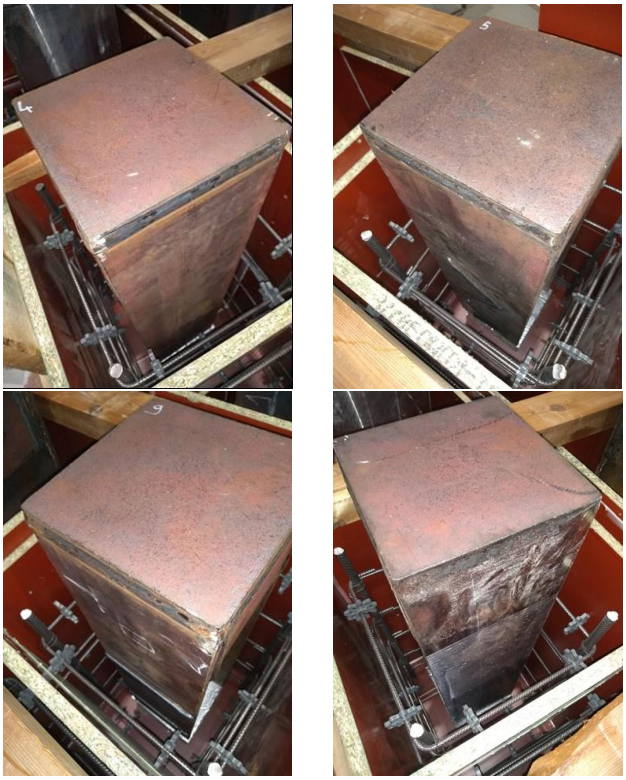

Figure 2 Test specimen surfaces: a) normal surface finishing, b) V-shaped ribs, c) I-shaped ribs, and d) ribbed surface.

For each specimen configuration, two loading types were used: short and long-term. Short-term tests are loaded after 28 days of concrete casting. One specimen/ configuration is tested 14 months after concrete casting. The specimen has been preloaded and kept in room conditions to evaluate the effect of concrete shrinkage on the quality of the bond properties.

The specimens are loaded with a hydraulic jack with a maximum capacity of 5000 kN. The test specimens are placed on a steel block. A reservation of 150mm at the bottom of the specimen allows for a possible free motion of the profile with respect to the concrete when the bond failure is reached.

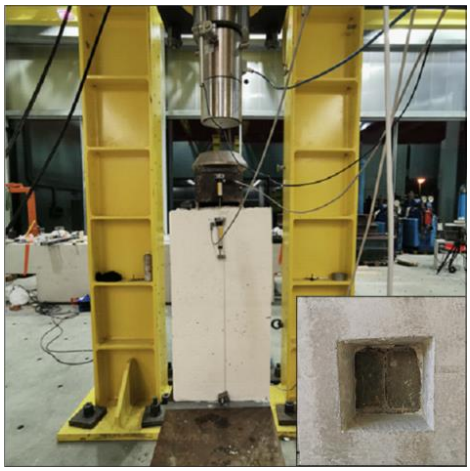

Figure 3 Test setup.

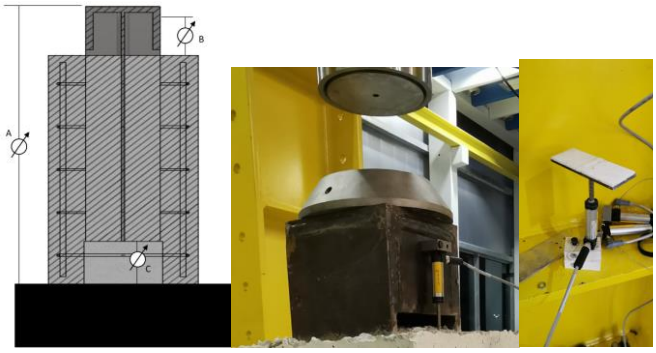

Figure 4 Instrumentation: a) Location of the displacement transducers; b) displacement transducer at the top of the specimen; c) displacement transducer at the bottom of the specimen.

The location of the instrumentation is presented in Fig. 4. The following measurements are recorded: total compression force applied on the specimen by the hydraulic jack; total displacement of the top of the profile (A); relative displacement between the profile and the top face of the concrete (B) and relative displacement between the profile and the concrete at the bottom of the profile, using the showed device, from which the white part is applied on the bottom plate of the profile (C).

For each configuration, 3 specimens in blue are tested in the short term, 28 days after concreting, and the red curve represents the specimen tested after 14 months. The comparisons are summarized in terms of top displacement, Fig. 5, and steel concrete relative displacement, Fig. 6, and Fig 7.

All curves are characterized by a two-stages behavior. The pre-peak behavior is characterized by the elastic performance of the system until the rupture of the mechanical bond resistance at the steel-concrete interface. The post-peak behavior is corresponding to friction behavior at the steel-concrete interface. The friction part is influenced by the type of interface and can be either horizontal and stable or slightly decreasing.

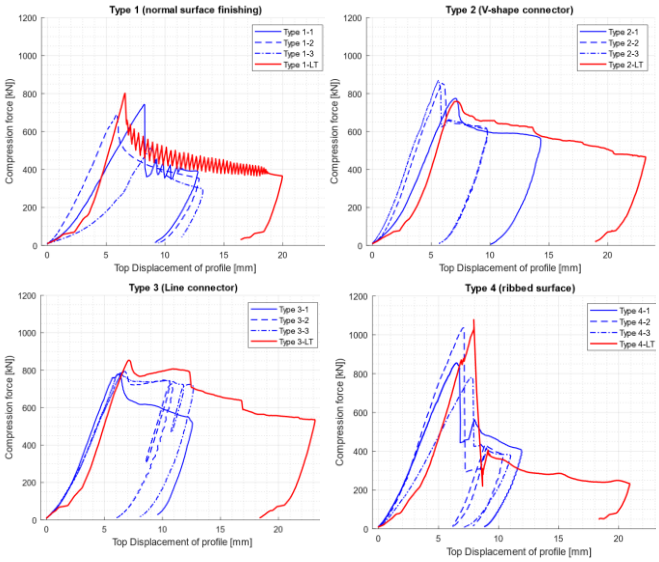

Figure 5 Top displacement of the profile: a) normal surface finishing, b) V-shaped ribs, c) I-shaped ribs, and d) ribbed surface.

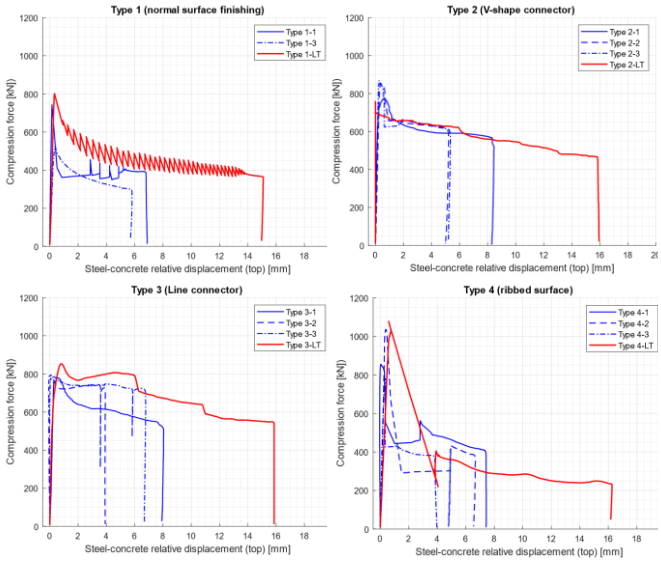

Figure 6 Steel concrete relative displacement (top): a) normal surface finishing, b) V-shaped ribs, c) I-shaped ribs, and d) ribbed surface.

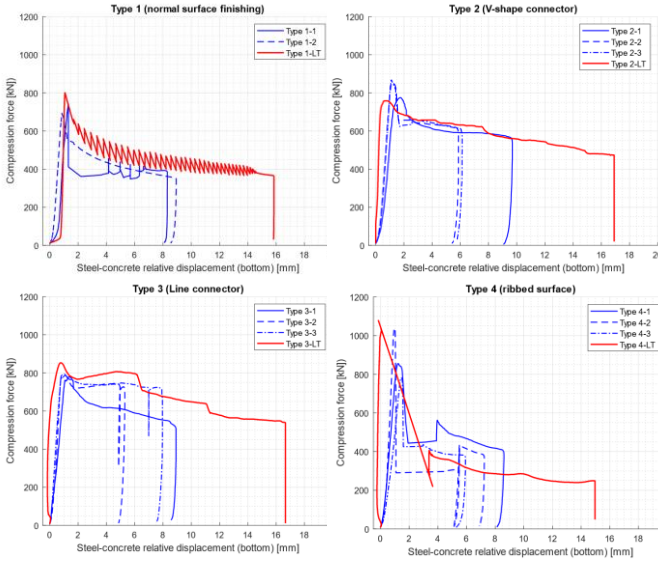

Figure 7 Steel concrete relative displacement (bottom): a) normal surface finishing, b) V-shaped ribs, c) I-shaped ribs, and d) ribbed surface.

Tables 2 - 5 presents a summary of the result obtained experimentally in terms of ultimate force and afferent slip. The results are compared in terms of force vs. global displacement (transducer A). Based on the average resistance per type and surface finishing, the 3 modified surfaces bring a significant improvement with respect to the normal situation. When compared with the reference configuration in terms of ultimate load, the best improvements are when using ribbed surface – 36%, while V-shaped and I-shaped ribs are increasing by 27% respectively 20%. V- and I-ribs lead to a much more stable resistance, with a COV of respectively 5% and 1%, compared to a COV of 12% and 14% for the normal or fully ribbed surface.

Due to the limited depth of the V and I-shaped ribs (8 mm), no diagonal cracks are observed through the thickness of the concrete. The behavior is rather controlled by the bond than by the development of a local strut and tie mechanism, as shown in Fig. 8. The only cases where through-thickness cracks are observed correspond to Type 2 (I ribs), as seen in Fig. 8c). In those cases, the inclination of the cracks is about 45°.

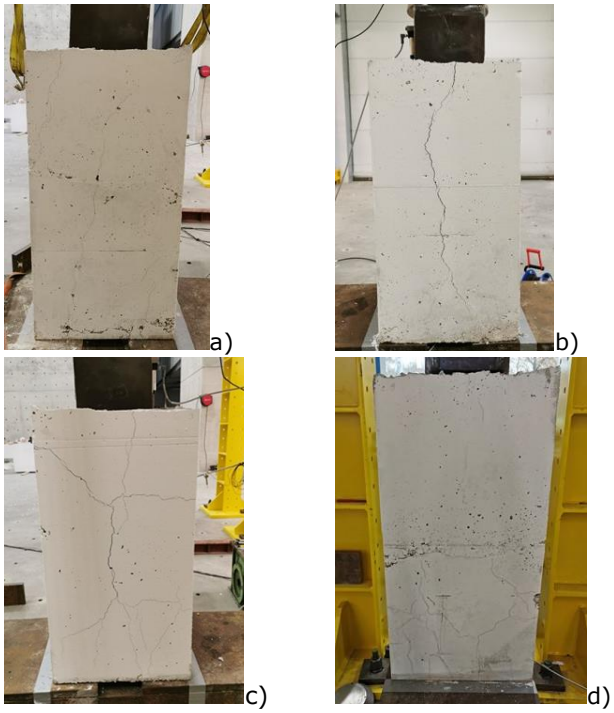

Figure 8 Post failure aspects of the specimens (short-term loading): a) normal surface finishing, b) V-shaped ribs, c) I-shaped ribs, and d) ribbed surface.

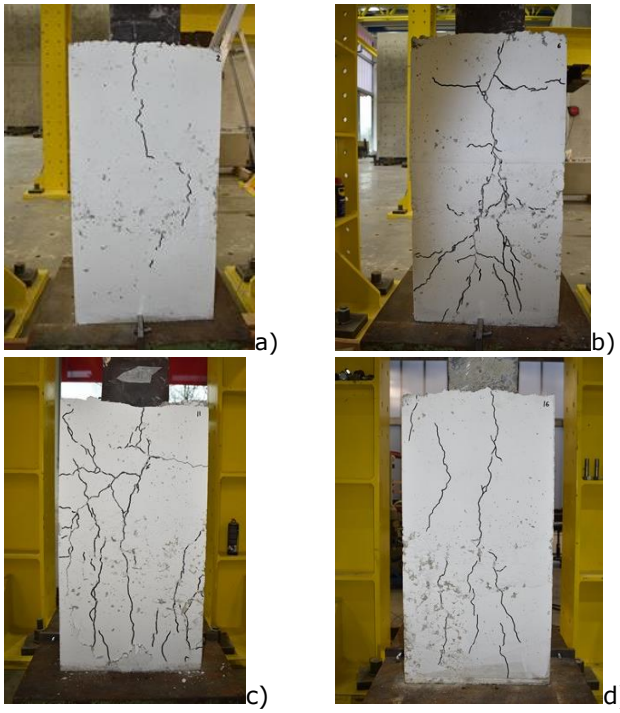

Figure 9 Post failure aspects of the specimens (long-term loading): a) normal surface finishing, b) V-shaped ribs, c) I-shaped ribs, and d) ribbed surface.

The compression force is converted into bond shear stress by dividing the average peak resistance by the profile embedded length times the external perimeter of the HEB 200 profile (i.e. 650 x 800 mm) [12]. The ribbed surface provides the highest shear bond resistance and is similar to the other rib types, as shown in Table 1.

Regarding long-term effects, no significant differences are observed between both phases of testing, i.e., the test results after shrinkage fall in the margin of variation of short-term tests. Also, the crack pattern remains similar, see Fig 9. Moreover, the long-term testing confirms the conclusions drawn after the short-term testing campaign.

Table 1 Bond shear resistance comparison.

Surface type	Bond shear resistance [N/mm²]	Ratio [%]
Normal surface	1.26	100%
V-shaped ribs	1.60	127%
I shaped ribs	1.51	120%
Ribbed surface	1.71	136%

Table 2 Normal surface finishing - Peak force values/ displacements.

	Peak [kN]	Δ at peak [mm]	Friction [kN]
Type 1-1	743	0.15	400
Type 1-2	694	-	400
Type 1-3	525	0.38	300
Type 1 average (COV %)	654 (14%)		
Type 1 LongTerm	802	0.33	400

Table 3 V shape finishing - Peak force values vs. displacements.

	Peak [kN]	Δ at peak [mm]	Friction [kN]
Type 2-1	775	0.63	600
Type 2-2	855	0.36	650
Type 2-3	868	0.29	650
Type 2 average (COV %)	833		
Type 2 - COV	5%		
Type 2 LongTerm	758	-	650

Table 4 I shape finishing - Peak force values vs. displacements.

	Peak [kN]	Δ at peak [mm]	Friction [kN]
Type 3-1	779	0.57	750
Type 3-2	794	0.05	750
Type 3-3	786	031	600
Type 3 average (COV %)	786 (1%)		
Type3LongTerm	853	0.80	800

Table 5 Multiple ribs - Peak force values vs. displacements.

	Peak [kN]	Δ at peak [mm]	Friction [kN]
Type 4-1	856	0.05	450
Type 4-2	1037	0.40	400
Type 4-3	781	0.34	300
Type 4 average (COV %)	891(12%)		
Type4LongTerm	1078	0.58	300

3 Numerical simulations of push-out tests

Abaqus® FEM software [13] has been used to create numerical models able to reproduce the behavior of the tested specimens. Concrete and steel profile parts were modeled using 8-node solid elements with reduced integration (C3D8R). The longitudinal and transversal reinforcement with 3D truss elements (T3D2). The truss elements were embedded in the eight-node solid element and a perfect bond was assumed. Cohesive behavior was defined between concrete and steel via zero-thickness cohesive material property. The damage evolution has a linear softening [14].

At the base of the specimen, only the z-axis degree of freedom is blocked. At the same time, the top surface of the steel profile was coupled with kinematic constraints on all DOF to the reference point, Fig. 10. The reference point at the top had released only the vertical movement DOF. In order to load the specimen, the reference point was pushed on z-axis to a maximum displacement. The size of the implemented mesh, especially in the contact zone, was related to the cohesive contact length.

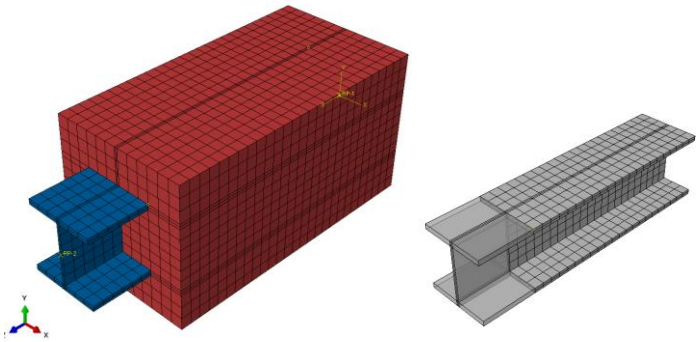

Figure 10 Numerical model with cohesive layer base on the steel profile mesh.

The application of the material laws was based on the European design codes [15] and experimental material tests. The concrete part is defined using Concrete Damage Plasticity (CDP) model having plasticity parameters Dilation Angle = 35°, Eccentricity = 0.1, fb0/fc0 = 1.16, Kc = 0.667 and Viscosity Parameter = 0.0001. Stress strain curves are defined as in Fib Model code [16] and presented in Fig 12 a)

For the steel profile, EN 1993-1-14 [17] was taken as a basis with a multilinear stress-strain curve as given in Fig. 11 b) with the modulus of elasticity of 210 GPa. For the horizontal and vertical reinforcement, the bilinear stress-strain curve was used in accordance with EN 1992-1-1. [18]

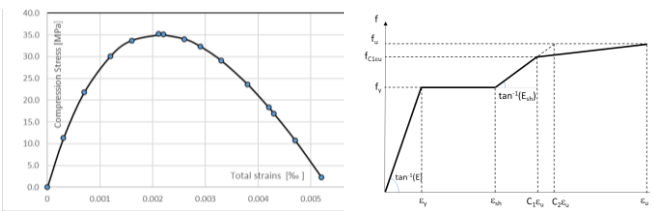

Figure 12 Material definition: a) concrete material; b) steel profile.

The comparisons in terms of load slip between the experimental results and numerical models are presented in Fig. 13. It can be observed that the numerical model is able to capture the behavior of the tested specimens. Only two configurations are represented, the reference and the I-rib specimen. The results confirm that the simplified model of cohesion can be used to capture the behavior of the newly studied shear connectors.

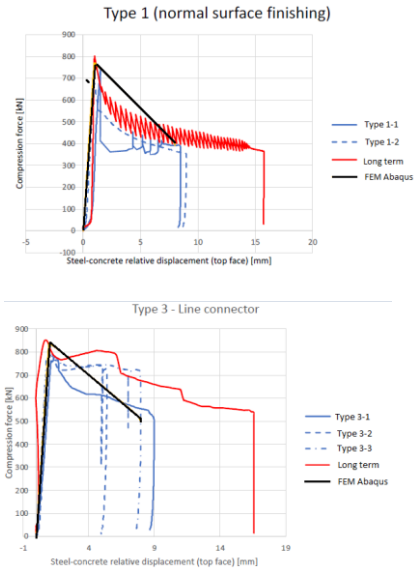

Figure 13 Load slip comparison in terms of steel concrete relative displacement (bottom): a) normal surface finishing, b) I-shaped ribs,

4 Shear resistance evaluation of I-shape rib

To evaluate the plate connector strength, a strut and tie model has been developed as shown in Fig. 11 [11], where the struts are assumed to be formed at an angle θ =45º.

For an HEB 200 S355 steel profile embedded in C30/37 concrete class, and a I-shape rib having the dimensions 8 x 200mm (a=8mm, b^* = 200mm), the strut resistance is equal to 33 kN.

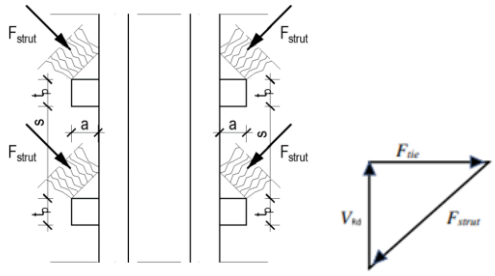

Figure 11 Strut and tie model to evaluate the rib connector strength.

The strut width is $\frac{a}{\cos\theta} = \frac{a}{\frac{\sqrt{2}}{2}} = 15.2mm$ (1)

The strut resistance is $F_{Rd} = \frac{a}{\sqrt{2}} \cdot \sigma_{Rd,max} \cdot b^* = 32.2\,kN.$ (2)

Where:

f_{cd}=20MPa, $\upsilon' = 1 - \frac{f_{ck}}{250} = 0.88$, $\sigma_{Rd,max} = 0.6 \cdot \upsilon' \cdot f_{cd} = 11MPa$

The strut resistance of one I shape rib is equal to:

$$V_{Rd,1plate} = F_{Rd} \cdot \cos\theta = 17kN \quad (3)$$

Compared with a shear connector Φ19 x 75 mm, in the same conditions, EC 4.1.- §6.6.3.1. (1) [15] gives the individual shear connector characteristic strength is equal with 81 kN.

5 Conclusions

The presented article deals with the characterization of new types of shear connectors dedicated to fully encased steel-concrete composite columns. Three new types of flat shear connectors have been proposed and analysed: V-shaped ribs, I-shaped ribs, and ribbed surface. The V and I shaped ribs have 8 mm each while the ribbed surface has 0.7 mm The performed investigation has been supported by the nominally identical reference tests without any mechanical shear connectors.

Short term loaded pushout tests showed that, in terms of ultimate load, the best improvements are when using ribbed surface – 36%, while V-shaped and I-shaped ribs are increasing by 27% respectively 20%. On another hand, V- and I-shape ribs lead to a much more stable resistance, with a COV of respectively 5% and 1%, compared to a COV of 12% and 14% for the normal or fully ribbed surface. Due to a limited height of the rib, the behaviour of the pushout specimens is controlled by the bond effects. Long term effects confirmed the behaviour in short term loading. Regarding long-term effects, no significant differences are observed between both phases of testing, they confirm the conclusions drawn after the short-term testing campaign.

Due to the simplicity of shape and similar behaviour with V- ribs, I shape ribs are used for further numerical simulations. Numerical models with a simplified definition of the cohesive behavior are meant to be used in a future work in which several parameters will be studied, like the influence of the I-rib height and its relationship with the steel profile size, the influence of the confinement effect by the longitudinal and vertical rebars and the concrete.

References

[1] H. Lungershausen, Zur Schubtragfähigkeit von Kopfbolzendübeln. Mitteilung Nr.88–7, Tech. rep., Institut für Konstruktiven Ingenieurbau, Ruhr-Universität Bochum,1988

[2] EN 1992-4, Eurocode 2: Design of concrete structures – Part 4: Design of fastenings for use in concrete, European Standard, European Committee for Standardization, Brussels, Belgium, 09.2016.

[3] K. Roik, G. Hanswille, Beitrag zur Bestimmung der Tragfähigkeit von Kopfbolzendübeln, Stahlbau, Volume 52, Issue 10, Ernst & Sohn, Berlin, 1983.

[4] Smart Composite Components - Concrete Structures Reinforced by Steel Profiles, SmartCoCo, European Commission, Research Programme of the Research Funds for Coal and Steel, TGS8, RFSR-CT-2012-00031, 2016.

[5] ANSI/AISC 360-16, American Institute of Steel Construction, Specification for Structural Steel Buildings. An American National Standard, 07.2016.

[6] J.C. Vianna, S.A.L. Andrade, P.C.G.S. Vellasco, L.F. Costa-Neves, Experimental study of perfobond shear connectors in composite construction, J Constr Steel Res 81 (62–75), 2013.

[7] G. Hanswille, M. Porsch, Lasteinleitung bei ausbetonierten Hohlprofil Verbundstützen, Stahlbau, Volume 73, Issue 9, Ernst & Sohn, Berlin, 2004.

[8] Chen L, Wang S, Experimental study on constitutive relationship between checkered steel and concrete, Construction and Building Materials (2019) 210 483-498

[9] D. Dragan and H. Degée, "Test Report on push-out tests of steel profiles with different surface finishing embedded in concrete "

[10] M. Chrzanowski, C. Odenbreit, R. Obiala, and T. Bogdan, Shear stresses analysis at the steel-concrete interface with the usage of bond eliminating products", XI Conference on Steel and Composite Construction, 2017, Portugal

[11] A. Plumier, D. Dragan, N.Q. Nguyen, H. Dgee, An analytical design method for steel-concrete hybrid walls, Structures, Vol. 9, February 2017, https://doi.org/10.1016/j.istruc.2016.12.007

[12] C. Roeder, R. Chmielowski and C. Brown, "Shear Connector Requirements for Embedded Steel Sections", Journal of Struc-tural Engineering, vol. 125, no. 2, pp. 142-151, 1999

[13] SIMULIA User Assistance. Abaqus, © Dassault Systèmes Simulia Corp. RI, USA: Pro-vidence; 2017.

[14] "Contact cohesive behavior", Abaqus-docs.mit.edu, 2022. [Online]. https://abaqus-docs.mit.edu/2017/English/SIMACAEITNRef-Map/simaitn-c-cohesivebehavior.htm

[15] EN 1994-1-1 Eurocode 4: Design of composite steel and concrete structures – Part 1-1: Genral rules and rules for buildings, European Standard, European Committee for Standardization, Brussels, Belgium.

[16] CEB -Fip Model Code 1990, Thomas Telford services, 1993.

[17] prEN 1993-1-14 3 Eurocode 3 - Design of Steel Structures - Part 1-14: Design Assisted by Finite Element Analysis.

[18] prEN 1992-1-1 Eurocode 2 - Design of Concrete Structures - Part 1-1: General rules and rules for buildings, December 2004.